Journal of Alloys and Compounds 509 (2011) 813–819

Contents lists available at ScienceDirect

Journal of Alloys and Compounds

journal homepage: www.elsevier.com/locate/jallcom

Effect of heat treatment on the microstructures and damping properties of biomedical Mg–Zr alloy

Ming-Hung Tsai[a,b,c], May-Show Chen[c,d,e], Ling-Hung Lin[e,f], Ming-Hong Lin[a], Ching-Zong Wu[e,f,**], Keng-Liang Ou[c,g,h,*], Chih-Hua Yu[c,h]

[a] Department of Mechanical Engineering and Graduate Institute of Mechanical and Precision Engineering, National Kaoshiung University of Applied Sciences, Kaoshiung 807, Taiwan
[b] Department of Dentistry, Chang Yin dental clinic, No.46-1, Yangming St., Banqiao City, Taipei County 220, Taiwan
[c] Research Center for Biomedical Devices, Taipei Medical University, Taipei 110, Taiwan
[d] School of Oral Hygiene, College of Oral Medicine, Taipei Medical University, Taipei 110, Taiwan
[e] Department of Dentistry, Taipei Medical University Hospital, Taipei 110, Taiwan
[f] School of Dentistry, College of Oral Medicine, Taipei Medical University, Taipei 110, Taiwan
[g] Graduated Institute of Biomedical Materials and Engineering, Taipei Medical University, Taipei 110, Taiwan
[h] Research Center for Biomedical Implants and Microsurgery Devices, Taipei Medical University, Taipei 110, Taiwan

ARTICLE INFO

Article history:
Received 11 June 2010
Received in revised form
16 September 2010
Accepted 18 September 2010
Available online 25 September 2010

Keywords:
Mg–Zr alloy
Microstructure
Twining
Damping capacity

ABSTRACT

In this study, we elucidated the effect of heat treatment on the microstructures and damping properties of the biomedical Mg–1 wt% Zr (K1) alloy by optical microscopy, transmission electron microscopy, energy-dispersive X-ray spectrometry, and experimental model analysis. The following microstructural transformation occurred when the as-quenched (AQ, i.e., solution heat treated and quenched) K1 alloy was subjected to aging treatment in the temperature range 200–500 °C: α-Mg → (α-Mg + $twin_{dense}$) → (α-Mg + $twin_{loose}$) → (α-Mg + α-Zr). This microstructural transformation was accompanied by variations in the damping capacity. The damping properties of the AQ K1 alloy subjected to aging treatment at 300 °C for 16 h were the best among those of the alloys investigated in the present study. The presence of twin structures in the alloy matrix was thought to play a crucial role in increasing the damping capacity of the K1 alloy. Hence, we state that a combination of solution treatment and aging is an effective means of improving the damping capacity of biomedical K1 alloys.

1. Introduction

The microstructures, mechanical properties, and corrosion resistance of Mg-based alloys have been studied widely by several researchers [1–5]. Addition of elemental Sr to Mg-based alloys results in grain refinement and improvement of the mechanical properties of the alloys [6]. Dong et al. [7] have reported that upon the addition of 7 wt% Y, the ultimate tensile strength and yield strength of the Mg–7Li alloy become 120% and 152% of those of the as-cast Mg–7Li alloy, respectively. Moreover, addition of alloying elements such as Al and rare-earth elements such as Nd, Re, and Pr to Mg-based alloys results in grain refinement, grain boundary strengthening, and solid-solution strengthening [8–11] and a consequent improvement of the corrosion resistance of the alloys. Such improved Mg-based alloys can be used for manufacturing aerospace components, automobile parts, electronic goods, and sports goods [12,13].

Recently, Mg-based alloys have been identified as potential implant materials because of their high biodegradability [14,15] and excellent mechanical properties such as high strength-to-density ratio and low elastic modulus (close to that of bone tissues) [16]. Previous in vivo studies have shown that Mg, which is an essential component of the enzyme system in humans, is a degradable biomaterial that can be used in medical implants [15]. Therefore, several Mg-based alloys, including Mg–Al–Li–Ce [10], Mg–Al–Zn (AZ31 and AZ91) [11,12], Mg–Zn [17], Mg–Ca [18], Mg–Zn–Mn [19], and Mg–Si–(Zn, Ca) [20], have been developed, and the feasibility of using these alloys in biomedical applications has been investigated.

The K1 alloy has recently attracted considerable attention because it has high specific damping capacity, excellent mechanical properties, and high biodegradability and biocompatibility, which make it suitable for use as an implant material [21–25]. Gu et al. [24] have reported that the addition of Zr helps in increasing the strength and decreasing the corrosion rate of the as-cast Mg–1Zr alloy. The results of hemocompatibility and cytotoxicity

* Corresponding author. Tel.: +886 2 27361661x5400; fax: +886 2 27395524.
** Corresponding author. Tel.: +886 2 27361661x5132.
E-mail addresses: chinaowu@tmu.edu.tw (C.-Z. Wu), klou@tmu.edu.tw (K.-L. Ou).

0925-8388/$ – see front matter © 2010 Elsevier B.V. All rights reserved.
doi:10.1016/j.jallcom.2010.09.098

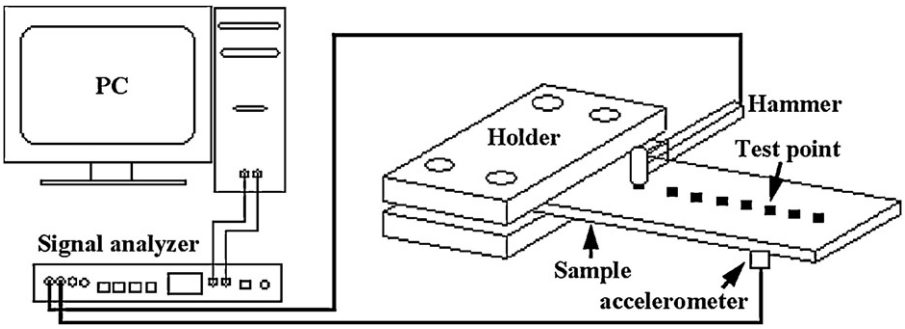

Fig. 1. Schematic diagram of the damping test system.

tests indicate that the Mg–1Zr alloy shows higher amount of adhered platelets and shows no significant toxicity to osteoblasts. Moreover, the Mg–1Zr alloy has higher specific damping capacity than do other metallic alloys [25] and hence is a promising candidate for a biomedical alloy.

The elastic modulus and damping capacity of metallic implants are two important factors that affect osseointegration [26–28]. Commonly used metallic implant materials, including titanium, stainless steel, and Co–Cr alloys, have a relatively higher elastic modulus than does natural bone tissue [16,29]. The high elastic modulus results in a strong stress-shielding effect, which reduces the stimulation of new bone growth and bone remodeling; as a consequence, the stability of the implant decreases [16,26]. The elastic modulus of pure Mg, Mg–Zr alloys, and other Mg-based alloys is low (40–50 GPa) [30,31] and is closer to that of natural bone tissues (10–30 GPa) [29] than are the elastic modulus of the currently used biomedical implant materials. Thus, the stress-shielding effect is suppressed in the case of pure Mg and Mg-based alloys. Moreover, the specific damping capacity of the Mg–Zr alloy (~80%) is considerably higher than that of AZ81A (~8%) and Mg–Cu–Mn alloys (~60%) [25,32]. Because of the high damping capacity, vibrations caused when the patient moves and the stress generated at the implant/bone interface are suppressed. As a result, the risk of bone tissue damage and loosening of the implant before biodegradation is reduced considerably [27,28], and the rate of osseointegration is enhanced. The purpose of the present study is to investigate the effect of heat treatment on the microstructures and damping properties of the biomedical Mg–1Zr alloy and provide valuable information on the use of this alloy in biomedical applications.

2. Experimental procedures

An 800-g pure-Mg melt was prepared in an electrical resistance furnace equipped with a graphite crucible; high-purity Mg was used for this purpose. The protective gas used was CO_2/0.5 vol.% SF_6. Pure Zr (1 wt%) was added to the melt at 750 °C, and manual stirring was carried out for 5 min by using a mild-steel cone ladle. The melt was allowed to settle for 15 min, and the resulting alloy was poured into 150 mm × 50 mm × 50 mm mild-steel molds and allowed to cool in a CO_2/0.5 vol.% SF_6 environment. The chemical composition of the alloy under investigation was confirmed to be Mg–0.55Zr by inductively coupled plasma-atomic emission spectrometry. The abovementioned composition was the average of the results obtained in 10 independent tests. After homogenization at 500 °C for 8 h in a protective Ar atmosphere, the ingots were cut into specimens of appropriate dimensions by using an electric spark linear cutting machine. The dimensions of the specimens used for heat treatment and damping measurements (bending beam specimens) were 10 mm × 10 mm × 2 mm and 130 mm × 10 mm × 3 mm, respectively. After solution heat treatment at 550 °C for 30 min, the specimens were quenched by immersing in room-temperature water. Aging treatment was carried out carefully in a vacuum furnace at temperatures ranging from 200 °C to 500 °C and for various periods; the aged samples were then quenched.

Specimens for optical microscopy (Olympus BX-51) studies were prepared by fine-wire cutting, chemical and electropolishing, and etching (etching solution: 3 ml HNO_3 + 20 ml CH_3COOH + 20 ml H_2O + 57 ml C_2H_4). Characterization of phases was performed in a JEOL-2100 transmission electron microscopy (TEM) equipped with an INCA energy dispersive X-ray spectrometer (EDS), operating at 200 kV. The average weight percentages of the alloying elements were determined by analyzing at least 10 different EDS spectra for each phase. Thin foils were electropolished to a thickness of around 40 μm and Ar-ion-milled by using a Gatan (model 691) precision ion polishing system until a hole was formed on the foil surface.

Damping tests were performed by experimental model analysis (or impulse-frequency response method) [33–35], in which the damping properties of a given material can be easily and rapidly evaluated. A schematic diagram of the damping test apparatus is shown in Fig. 1. Test specimens were fabricated by using a cantilever beam structure. An impact hammer (actuator) and an accelerometer (sensor) were used to excite the specimens and measure the frequency response functions (FRFs), respectively. The impact hammer was aimed at 10 test points distributed on the surface of the specimens. The corresponding 10 sets of FRFs were combined and processed for curve fitting by using CADAPC to obtain the characteristic frequencies (f) and damping coefficients (ξ) of the specimens.

3. Results and discussion

Fig. 2 shows the optical micrograph of the AQ K1 alloy, it is clear that the microstructure consists of α-Mg grains. Optical microscopy images show that there are no other precipitates or intermetallic compounds in the matrix. These results confirm the complete dissolution of Zr in the α-Mg matrix during solution heat treatment. The microstructural characteristics of AQ K1 are similar to those of Mg–0.6 wt% Zr [36]. The average grain size of AQ K1 is calculated to be approximately 96.4 μm by using an OmniMet imaging system. Fig. 3 presents the damping properties of the AQ K1 alloy. From the 10 sets of FRFs, an average FRF plot is obtained for the AQ K1 alloy, as shown in Fig. 3(a). The solid and dashed lines represent the experimental and synthesized values, respectively. The good agreement between these two sets of values is indicative of the reliability of the experimental approach employed. The average f and ξ values of AQ K1 are 485 Hz and 0.0832, respectively. The ξ value of AQ K1 is

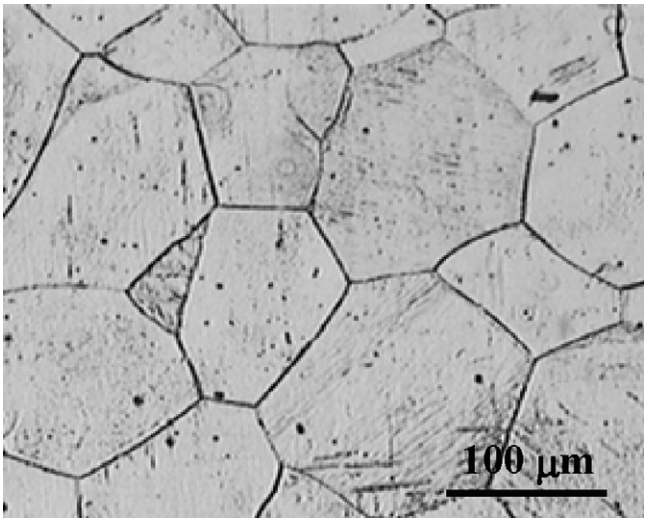

Fig. 2. Optical micrograph of the AQ K1 alloy.

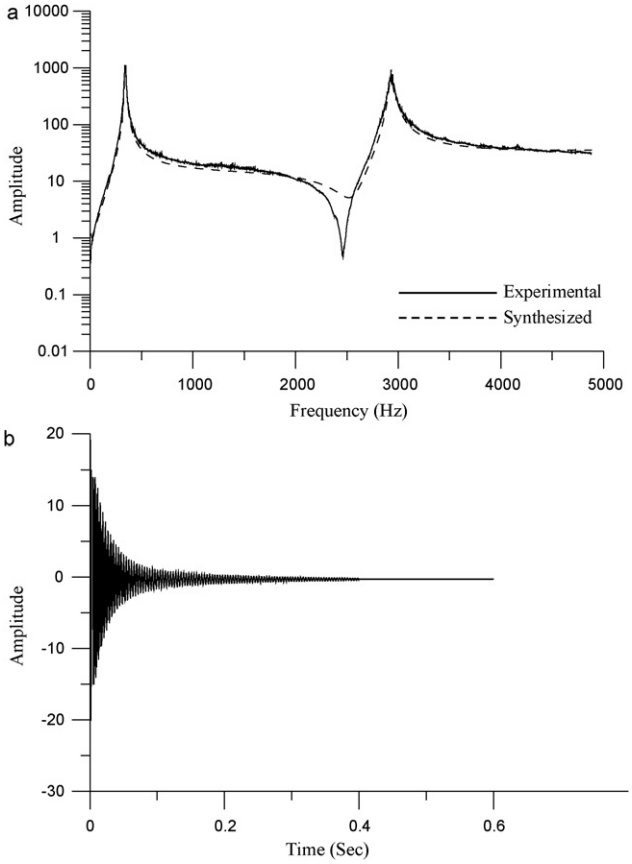

Fig. 3. Damping properties of the AQ K1 alloy: (a) an average FRF diagram and (b) logarithmic decrement diagram.

approximately 4.4 times that of the Ti–4.8Al–2.5Mo–1.4 V alloy [34] and 3.5 times that of the Ti–6Al–4V alloy [35]. It is known that alloys with a high ξ value have high damping capacity. Fig. 3(b) shows the logarithmic decrement diagram for the AQ K1 alloy. Amplitude dissipation occurs in approximately 0.4 s when the hammer impacts the specimen. This rapid amplitude decay implies that the specimen has a good damping capacity.

The microstructural characteristics of AQ K1 remained similar to those shown in Fig. 2 even after the alloy was subjected to aging treatment at 200 °C for various periods. Only the grain sizes of the α-Mg phase showed a slight change with the soaking time. The optical micrograph of the AQ K1 alloy aged at 200 °C for 16 h clearly revealed that the microstructure comprised a single phase, α-Mg (Fig. 4). No other precipitates could be detected in the matrix by optical microscopy observations. The damping test results indicated that there were no significant differences in the damping properties as compared with AQ K1 alloy. The average f and ξ values of the AQ K1 alloy aged at 200 °C for various periods were in the range 481–510 Hz and 0.0811–0.0876, respectively.

The microstructure and damping properties of the AQ K1 alloy subjected to aging treatment at 300 °C for a short period (<4 h) were similar to those of AQ K1 alloy and the AQ K1 alloy aged at 200 °C. When the soaking time was increased to 8 h, some twin structures were formed in the α-Mg grains (as indicated by the arrows) [37], as shown in Fig. 5(a). The number of twins increased with the soaking time. Fig. 5(b) presents the optical micrograph of the AQ K1 alloy aged at 300 °C for 16 h. It was clear that a high density of twins were formed in the α-Mg matrix [38]. Fig. 6 shows the damping properties of the AQ K1 alloy aged at 300 °C for 8 h and 16 h. The average FRF plots of the two samples revealed the high reliability of the test results obtained (Fig. 6(a) and (b)). The average ξ value of the AQ K1 alloy aged at 300 °C for 16 h was higher than that of the alloy aged at 300 °C for 8 h and AQ state. The average ξ values of the AQ K1 alloy aged at 300 °C for 8 h and 16 h were 0.1134 and 0.1724, respectively. It has been stated that an alloy with a low f may have a high ξ value [34]. The f values of the AQ K1 alloy aged at 300 °C for 8 h and

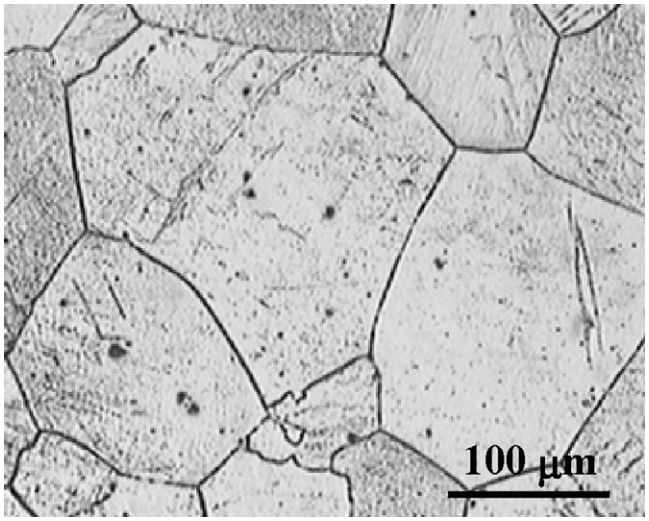

Fig. 4. Optical micrograph of the AQ K1 alloy aged at 200 °C for 16 h.

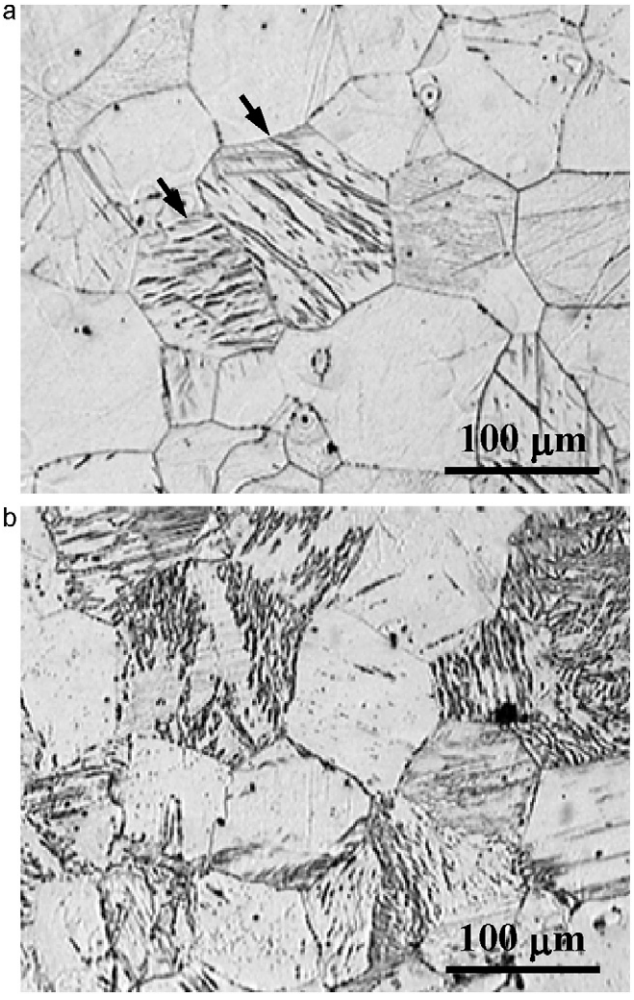

Fig. 5. Optical micrograph of the AQ K1 alloy aged at 300 °C for (a) 8 h and (b) 16 h.

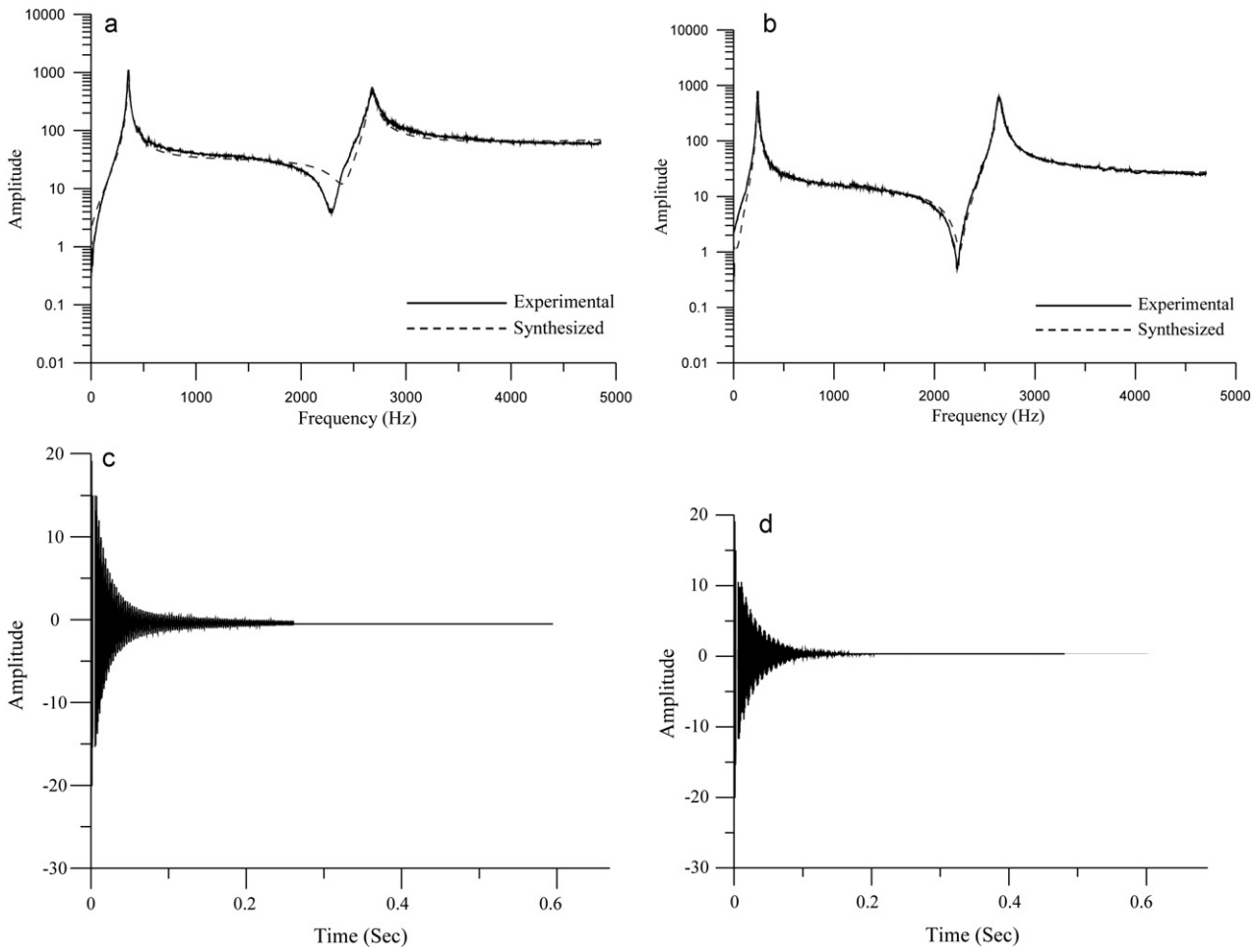

Fig. 6. Damping properties of the AQ K1 alloy aged at 300 °C for 8 h and 16 h, respectively: (a) an average FRF diagram (8 h), (b) an average FRF diagram (16 h), (c) logarithmic decrement diagram (8 h) and (d) logarithmic decrement diagram (16 h).

16 h were 451 Hz and 380 Hz, respectively. Fig. 6(c) and (d) depicts the logarithmic decrement diagrams of the abovementioned two samples. Apparently, the amplitude decay time was shorter in the case of the AQ K1 alloy aged at 300 °C for 16 h (0.15 s) than in the case of the alloy aged at 300 °C for 8 h (0.25 s). This result strongly demonstrated that the presence of twin structures plays a crucial role in increasing the damping capacity of K1 alloys.

There was no significant difference between the microstructures and damping properties of the AQ K1 alloy aged at 400 °C for 4 h and that aged at 300 °C for 16 h. However, when the soaking time was prolonged to 8 h, coarse and loose twin structures were formed in the α-Mg grains, as shown in Fig. 7. The presence of such twin structures contributed to the degradation of the damping properties of the alloy. The average f and ξ values of the AQ K1 alloy aged at 400 °C for 8 h were 467 Hz and 0.0956, respectively. Moreover, the amplitude decay time in the case of the K1 alloy with coarse and loose twin structures was found to be 0.31 s. Similar results were observed for the AQ K1 alloy aged at 400 °C for 16 h.

When the aging temperature was increased to 500 °C, a microstructural transition occurred in the matrix of the K1 alloy. Fig. 8(a) shows the optical micrograph of the AQ K1 alloy aged at 500 °C for 4 h. Clearly, some island-like phases (indicated by the arrows) were formed in the matrix and at the grain boundaries. This microstructural feature was similar to that of Mg–0.54 wt% Zr homogenized at 380 °C for 12 h [39]. When the soaking time was prolonged to 16 h, the amounts of the island-like phases increased significantly, as illustrated in Fig. 8(b). Therefore, the microstructure of the AQ K1 alloy aged at 500 °C for various periods comprised the α-Mg phase and island-like phases. The results of damping tests revealed that the damping properties of the AQ K1 alloy aged at 500 °C for 4 h were similar to those of the K1 alloy aged at 400 °C for 8 h. From Fig. 9, it could be seen that the average f and ξ values of the AQ K1 alloy aged at 500 °C for 16 h were 470 Hz and 0.0895, respectively. The ξ value of this alloy was between the ξ values of

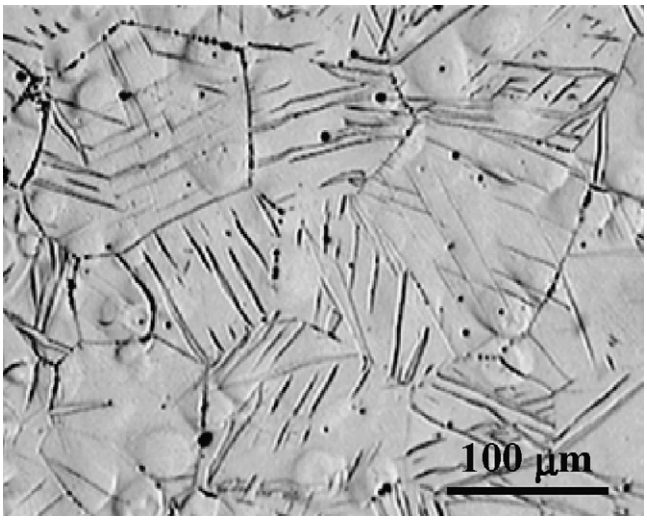

Fig. 7. Optical micrograph of the AQ K1 alloy aged at 400 °C for 8 h.

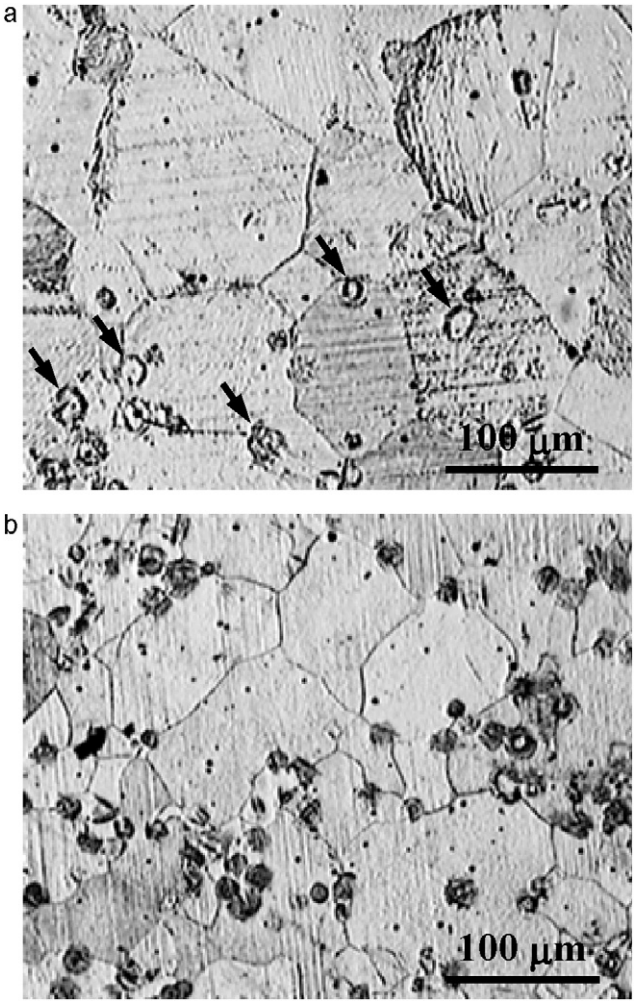

Fig. 8. Optical micrograph of the AQ K1 alloy aged at 500 °C for (a) 4 h and (b) 16 h.

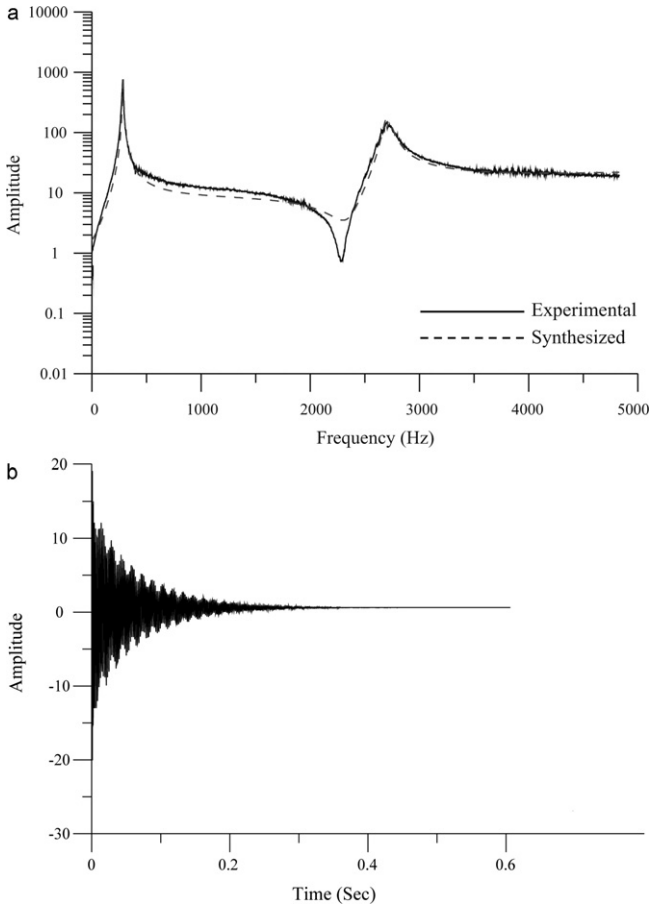

Fig. 9. Damping properties of the AQ K1 alloy aged at 500 °C for 16 h: (a) an average FRF diagram and (b) logarithmic decrement diagram.

AQ K1 alloy and the AQ K1 alloy aged at 400 °C for 8 h. Moreover, the amplitude decay time in the case of the K1 alloy containing island-like phases was found to be approximately 0.36 s. Thus, we concluded that the island-like phases have no significant influence on the damping properties of the K1 alloy.

In order to clarify the relationship between the damping properties and the microstructure of the heat-treated K1 alloy, the specimen was further analyzed by TEM. Fig. 10 presents a bright-field (BF) image of the matrix in the $[\bar{2}\,4\,\bar{2}\,3]$ zone of the AQ K1 alloy. This image revealed that the matrix comprised only the α-Mg phase with a hexagonal-close-packed (HCP) structure [37,40]. No other precipitates could be found in the matrix. A similar result was obtained for the AQ K1 alloy aged at 200 °C for various periods. Fig. 11 shows a BF image of the AQ K1 alloy aged at 300 °C for 8 h, which was taken from the matrix in the [0 0 0 1] zone, indicating that in addition to the α-Mg spots, twin spots coexist in the selected-area electron diffraction pattern (SAEDP). The BF image clearly showed the presence of twin structures in the matrix. This microstructural feature corresponded to that shown in Fig. 5(a). Similar twin structures were seen in the matrix of the AQ K1 alloy aged at 400 °C for 8 h. Fig. 12(a) shows a BF image of the matrix in the [0 0 0 1] zone of the AQ K1 alloy aged at 500 °C for 16 h. Some island-like phases were observed in the matrix. The SAEDPs revealed the presence of α-Mg spots as well as small superlattice spots. On the basis of the camera length and *d*-spacing between the superlattice spots and the results of EDS analysis (as shown in Fig. 12(b)), the spots were confirmed to correspond to the α-Zr phase having an HCP structure; the lattice parameters were $a = 3.23$ Å and $c = 5.14$ Å [40]. Therefore, when the AQ K1 alloy was subjected to aging treatment in the temperature range 200–500 °C, microstructural transformation occurred via the following sequence: α-Mg → (α-Mg + $\text{twin}_{\text{dense}}$) → (α-Mg + $\text{twin}_{\text{loose}}$) → (α-Mg + α-Zr).

The results deduced on the basis of the abovementioned observations are discussed here. In the case of metallic alloys, the

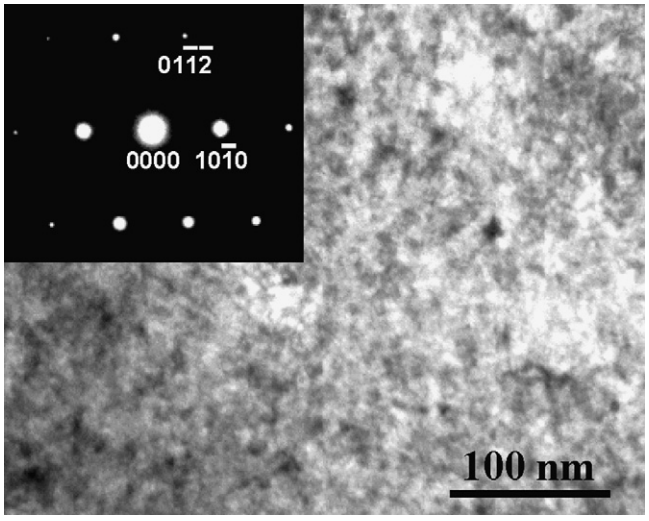

Fig. 10. BF image of the AQ K1 alloy, which was taken from the matrix in the $[\bar{2}\,4\,\bar{2}\,3]$ zone.

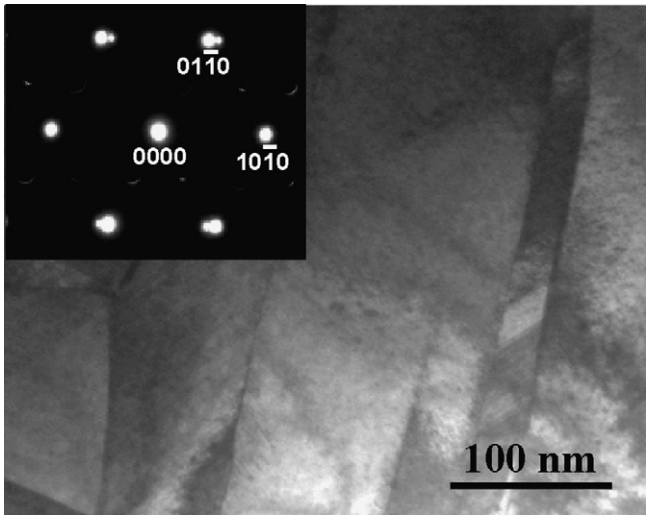

Fig. 11. BF image of the AQ K1 alloy aged at 300 °C for 8 h, which was taken from the matrix in the [0 0 0 1] zone.

damping properties may be increased from the thermoelastic damping, magnetic damping, viscous damping, and defect damping [41]. In conventional crystalline materials, defect damping contributes significantly to the overall damping properties [42]. Material damping is extremely sensitive to the presence of defects.

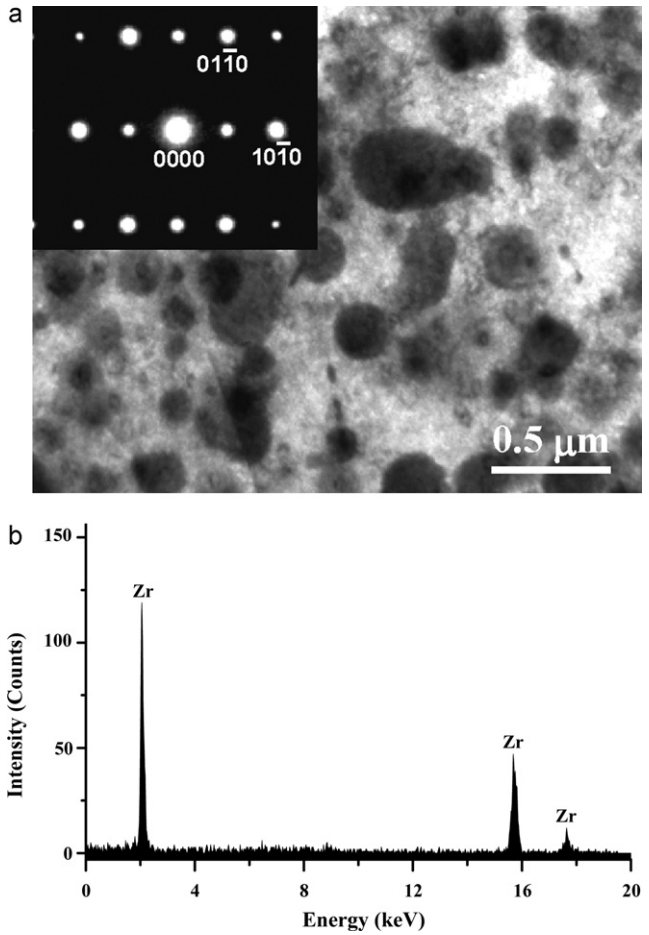

Fig. 12. (a) BF image of the AQ K1 alloy aged at 500 °C for 16 h, which was taken from the matrix in the [0 0 0 1] zone and (b) EDS spectrum taken from the island-like phase in (a).

The intrinsic movement of defects (of any type) under applied cyclic stress may give rise to internal friction, which in turn would cause energy dissipation. Four common types of defects are observed in polycrystalline metallic alloys: point defects, line defects, surface defects, and bulk defects [42]. The damping mechanism associated with each of these defects is different. From Fig. 5(b), it is apparent that twin structures are present in the matrix of the alloy. The damping mechanism, which is responsible for vibration suppression, is similar for twin structures and surface defects, i.e., movement of the internal twin boundaries in the α-Mg grains and resultant internal friction [25]. Twinning may enhance the rate of grain boundary sliding when new slip systems are activated after reorientation of the lattice atoms in the twinned areas [43]. Moreover, a high density of twins may result in the formation of a large number of interface boundaries in the grains. Ustinov et al. [44] reported that the dissipative properties of nanotwinned Cu are mainly determined by the nature of the twinned substructures. With an increase in the twin boundary density, the nonlinear amplitude dependence of the logarithmic decrement becomes almost linear. Therefore, a high density of twin structures leads to rapid and marked enhancement of the damping capacity. Hence, it is reasonable to state that the twin structures play a crucial role in increasing the damping capacity of the K1 alloy. More tests must be carried out on the microstructural characteristics, mechanical properties, cytotoxicity, and biocompatibility of the K1 alloy before it is used in clinical applications.

4. Conclusions

There was no notable difference in the microstructure and damping properties of the AQ K1 alloy before and after aging treatment at 200 °C. When the AQ K1 alloy was subjected to aging treatment at 300 °C for 8 h, some twins were formed in the α-Mg grains. Moreover, the number of twins increased with the soaking period. The AQ K1 alloy aged at 300 °C for 16 h had the best damping properties among all the samples considered in this study. The average f and ξ values of this alloy were 380 Hz and 0.1724, respectively. When the AQ K1 alloy was aged at 400 °C, coarse and loose twin structures were formed within the α-Mg grains. These twin structures caused degradation of the damping properties of the alloy. Upon aging at temperatures higher than 500 °C, the microstructure of this alloy was found to comprise both α-Mg and α-Zr phases. However, the α-Zr phase had no significant influence on the damping properties of the K1 alloy.

Acknowledgements

The authors would like to thank the Center of Excellence for Clinical Trial and Research in Neurology and Neurosurgery, Taipei Medical University-Wan Fang Hospital for financially supporting this research under contract No. DOH99-TD-B-111-003 and supported partly by Alliance Global Technology Co., LTD.

References

[1] M. Sun, G. Wu, J. Dai, W. Wang, W. Ding, J. Alloys Compd. 494 (2010) 426.
[2] B. Jiang, D. Qiu, M.-X. Zhang, P.D. Ding, L. Gao, J. Alloys Compd. 492 (2010) 95.
[3] J. Gubicza, K. Máthis, Z. Hegedűs, G. Ribárik, A.L. Tóth, J. Alloys Compd. 492 (2010) 166.
[4] E.N. El Sawy, H.A. El-Sayed, H.A. El Shayeb, J. Alloys Compd. 492 (2010) 69.
[5] L. Wang, T. Shinohara, B.-P. Zhang, J. Alloys Compd. 496 (2010) 500.
[6] H. Liu, Y. Chen, H. Zhao, S. Wei, W. Gao, J. Alloys Compd. 504 (2010) 345.
[7] H. Dong, L. Wang, Y. Wu, L. Wang, J. Alloys Compd. 506 (2010) 468.
[8] Z. Wen, C. Wu, C. Dai, F. Yang, J. Alloys Compd. 488 (2009) 392.
[9] J. Zhang, K. Liu, D. Fang, X. Qiu, P. Yu, D. Tang, J. Meng, J. Alloys Compd. 480 (2009) 810.
[10] L. Gao, C. Zhang, M. Zhang, X. Huang, N. Sheng, J. Alloys Compd. 468 (2009) 285.
[11] J. Zhang, J. Wang, X. Qiu, D. Zhang, Z. Tian, X. Niu, D. Tang, J. Meng, J. Alloys Compd. 464 (2008) 556.

[12] B.L. Mordike, T. Ebert, Mater. Sci. Eng. A 302 (2001) 37.
[13] T. Kaneko, M. Suzuki, Mater. Sci. Forum 419–422 (2003) 67.
[14] F. Witte, J. Fischer, J. Nellesen, H.-A. Crostack, V. Kaese, A. Pisch, Biomaterials 27 (2006) 1013.
[15] F. Witte, V. Kaese, H. Haferkamp, E. Switzer, A. Meyer-Lindenberg, C.J. Wirth, H. Windhagen, Biomaterials 26 (2005) 3557.
[16] M.P. Staiger, A.M. Pietak, J. Huadmai, G. Dias, Biomaterials 27 (2006) 1728.
[17] S. Zhang, J. Li, Y. Song, C. Zhao, X. Zhang, C. Xie, Y. Zhang, H. Tao, Y. He, Y. Jiang, Y. Bian, Mater. Sci. Eng. C 29 (2009) 1907.
[18] Z. Li, X. Gu, S. Lou, Y.F. Zheng, Biomaterials 29 (2008) 1329.
[19] E. Zhang, D. Yin, L. Xu, L. Yang, K. Yang, Mater. Sci. Eng. C 29 (2009) 987.
[20] E. Zhang, L. Yang, J. Xu, H. Chen, Acta Biomater. 6 (2010) 1756.
[21] M. Qian, Acta Mater. 55 (2007) 943.
[22] M. Qian, Acta Mater. 54 (2006) 2241.
[23] F. Witte, N. Hort, C. Vogt, S. Cohen, K.U. Kainer, R. Willumeit, F. Feyerabend, Curr. Opin. Solid State Mater. Sci. 12 (2008) 63.
[24] X. Gu, Y. Zheng, Y. Cheng, S. Zhong, T. Xi, Biomaterials 30 (2009) 484.
[25] S.H. Baik, Nucl. Eng. Des. 198 (2000) 241.
[26] J. Nagels, M. Stokdijk, P.M. Rozing, J. Shoulder Elbow Surg. 12 (2003) 35.
[27] P.L.S. Li, N.B. Jones, P.J. Gregg, Med. Eng. Phys. 18 (7) (1996) 596.
[28] M.B. Nasab, M.R. Hassan, Trends Biomater. Artif. Organs 24 (1) (2010) 69.
[29] M. Long, H.J. Rack, Biomaterials 19 (1998) 1621.
[30] T. Sumitomo, C.H. Cáceres, M. Veidt, J. Light Met. 2 (2002) 49.
[31] S. Ganeshan, S.L. Shang, Y. Wang, Z.-K. Liu, Acta Mater. 57 (2009) 3876.
[32] K. Nishiyamaa, R. Matsui, Y. Ikeda, S. Niwa, T. Sakaguchid, J. Alloys Compd. 355 (2003) 22.
[33] B.T. Wang, Mech. Syst. Signal Process. 12 (5) (1998) 627.
[34] P.W. Peng, K.L. Ou, C.Y. Chao, Y.N. Pan, C.H. Wang, J. Alloys Compd. 490 (2010) 661.
[35] D.G. Lee, S. Lee, Y. Lee, Mater. Sci. Eng. A 486 (2008) 19.
[36] D.Q.J. Wan, C. Wang, G.C. Yang, Mater. Sci. Eng. A 517 (2009) 114.
[37] L. Capolungoa, I.J. Beyerlein, G.C. Kaschner, C.N. Tomé, Mater. Sci. Eng. A 513–514 (2009) 42.
[38] L. Čížek, L. Pawlica, R. Kocich, M. Janošec, T. Tański, M. Praźmowski, J. Arch. Mater. Manuf. Eng. 27 (2008) 127.
[39] Z. Luo, S. Zhang, Acta Metall. Sin. 6 (1993) 337.
[40] G.L. Liu, Acta Phys. Sin. 57 (1043) (2008) (in Chinese).
[41] Z.M. Zhang, J.H. Wang, G.C. Yang, Y.O. Zhou, J. Mater. Sci. 35 (2000) 3383.
[42] I.G. Ritchie, Z.-L. Pan, Metall. Trans. A 22A (1991) 607.
[43] L. Lin, W. Wu, Y. Lin, L. Chen, Z. Liu, J. Mater. Sci. 41 (2006) 409.
[44] A.I. Ustinov, V.S. Skorodzievski, E.V. Fesiun, Acta Mater. 56 (2008) 3770.